Computer simulations of nematic drops: Coupling between drop shape and nematic order

L. F. Rull, J. M. Romero-Enrique, and A. Fernandez-Nieves

Citation: The Journal of Chemical Physics **137**, 034505 (2012); doi: 10.1063/1.4733974
View online: http://dx.doi.org/10.1063/1.4733974
View Table of Contents: http://scitation.aip.org/content/aip/journal/jcp/137/3?ver=pdfcov
Published by the AIP Publishing

Computer simulations of nematic drops: Coupling between drop shape and nematic order

L. F. Rull,[1] J. M. Romero-Enrique,[1] and A. Fernandez-Nieves[2]
[1]*Departamento de Física Atómica, Molecular y Nuclear, Área de Física Teórica, Universidad de Sevilla, Apartado de Correos 1065, 41080 Sevilla, Spain*
[2]*School of Physics, Georgia Institute of Technology, Atlanta, Georgia 30339-0430, USA*

(Received 31 January 2012; accepted 22 June 2012; published online 17 July 2012)

We perform Monte Carlo computer simulations of nematic drops in equilibrium with their vapor using a Gay-Berne interaction between the rod-like molecules. To generate the drops, we initially perform *NPT* simulations close to the nematic-vapor coexistence region, allow the system to equilibrate and subsequently induce a sudden volume expansion, followed with NVT simulations. The resultant drops coexist with their vapor and are generally not spherical but elongated, have the rod-like particles tangentially aligned at the surface and an overall nematic orientation along the main axis of the drop. We find that the drop eccentricity increases with increasing molecular elongation, κ. For small κ the nematic texture in the drop is bipolar with two surface defects, or boojums, maximizing their distance along this same axis. For sufficiently high κ, the shape of the drop becomes singular in the vicinity of the defects, and there is a crossover to an almost homogeneous texture; this reflects a transition from a spheroidal to a spindle-like drop. © *2012 American Institute of Physics*. [http://dx.doi.org/10.1063/1.4733974]

I. INTRODUCTION

Drops of nematic liquid crystal form the basis of many privacy windows and other electro-optic devices. Examples include polymer dispersed liquid crystals, which are able to switch between scattering and transparent states after application of an external electric field,[1] and holographic polymer dispersed liquid crystals, which are based on an organized distribution of the drops and can switch between diffracting and transparent states.[2–5]

Drops of nematic liquid crystal are also fascinating systems where geometrical frustration is at play; the topological constraints imposed by the spherical-like shape of the drop prevent the local order favored by physical interactions from being maintained everywhere in the drop. As a result, there are defects in the order, which are spatial regions where the nematic director is undefined. There are many possible configurations for either tangential or perpendicular alignment of the rod-like molecules at the bounding surface,[1] and it is minimization of the free energy which ultimately determines the nematic arrangement in the drop and thus the number and type of defects that characterizes it. In some situations, the shape of the drop is fixed, because the surrounding media is polymerized. In addition, even if this is not the case, surface tension tends to make everything spherical. However, since the seminal work by Bernal and Fankuchen on plant virus tactoids[6] there is experimental evidence indicating that the shape of a nematic drop can change either if it is small enough[7] or if external electric fields are applied;[8] this suggests an interesting interplay between minimization of the free energy and the shape of the drop. Continuum theory has been extensively applied in the literature to predict the shape of nematic drops.[9–16] It is essentially the ratio between surface and elastic energies, $\Delta = \gamma V^{1/3}/K$, with K a bulk Frank elastic constant, γ the interfacial tension of the coexisting phases, and V the volume of the drop, what determines whether the drops remain spherical or not. For $\Delta < 1$, drops are elongated, while for $\Delta \gg 1$, they are spherical. Additionally, the nematic texture in the drop is governed by the surface anchoring strength ω, which measures the anisotropy of surface tension with respect to the nematic surface anchoring, if tangential anchoring is favored.[15,16] For small ω, there is no preference in the anchoring direction and the nematic texture is almost homogeneous, having no defects in the ordering; only for small Δ may the surface develop cusps, which are points on the surface with undefined curvature. For large ω, there is a strong preference for tangential anchoring and the nematic texture becomes bipolar. The nematic configuration is characterized, in this case, by the presence of two point defects on the surface, referred to as boojums, which maximize their distance by locating themselves a drop diameter away from each other.

Formation of drops of spherical particles interacting with a Lennard-Jones potential has been extensively studied theoretically[17,18] and by computer simulations since the pioneering work of Thompson *et al.*,[19] see for instance.[20–27] In the case of nematic drops, most computer simulations are performed on spherical nematic drops.[28–31] The shape is imposed and is not allowed to change. However, computer simulations addressing the formation of nematic drops in monocomponent nematogens in equilibrium with its vapor and from binary mixtures of spherical and rod-like particles indicate that the drops are non-spherical.[32–36] Despite these results are suggestive of the interplay between nematic order and drop shape, this relationship still remains to be explored in the absence of external forces.

In this paper, we perform computer simulations of a Gay-Berne fluid in the nematic-vapor coexistence region,

where nematic drops coexist with their vapor, and correlate the nematic order inside the drops with their shape. We evaluate the inertial tensor of the drops and their order parameter and describe the results for different values of the molecular elongation, κ, defined as the ratio between the center-to-center distance between the rod-like molecules in the end-to-end and side-by-side configurations. Since the phase behavior of the Gay-Berne fluid is only well documented for $\kappa = 3$,[37] we perform additional "zero-pressure" simulations to obtain nematic-vapor coexistence regions at higher κ. Our results open new ways to generate nematic drops for further simulation studies.

II. COMPUTER SIMULATIONS

A. Previous simulation results with Gay-Berne interactions

The Gay-Berne potential[38] is the most common generalization of the Lennard-Jones potential for describing the interaction between rod-like particles:

$$U_{ij}(\mathbf{r}_{ij}, \mathbf{u}_i, \mathbf{u}_j) = 4\varepsilon(\hat{\mathbf{r}}_{ij}, \mathbf{u}_i, \mathbf{u}_j)\left[\rho_{ij}^{-12} - \rho_{ij}^{-6}\right], \quad (1)$$

where

$$\rho_{ij} = \frac{r_{ij} - \sigma(\hat{\mathbf{r}}_{ij}, \mathbf{u}_i, \mathbf{u}_j) + \sigma_0}{\sigma_0} \quad (2)$$

with $\mathbf{u}_i$ the unit vector along the symmetry axis of particle i, $r_{ij} = |\mathbf{r}_i - \mathbf{r}_j|$ the distance along the intermolecular vector $\mathbf{r}_{ij}$ joining the centers of mass of particles i and j, and $\hat{\mathbf{r}}_{ij} = \mathbf{r}_{ij}/r_{ij}$. The anisotropic contact distance, $\sigma(\hat{\mathbf{r}}_{ij}, \mathbf{u}_i, \mathbf{u}_j)$, and the depth of the interaction energy, $\varepsilon(\hat{\mathbf{r}}_{ij}, \mathbf{u}_i, \mathbf{u}_j)$, depend on the orientational unit vectors, the length-to-breadth ratio of the particle, $\kappa = \sigma_{ee}/\sigma_{ss}$, and the energy depth anisotropy, $\kappa' = \epsilon_{ee}/\epsilon_{ss}$, which are both defined as the ratio of the size and energy interaction parameters in the end-to-end (ee) and side-by-side (ss) configurations, respectively. Their expressions are given in terms of an arbitrary length scale, σ_0, and an arbitrary energy scale, ϵ_0:

$$\frac{\sigma(\hat{\mathbf{r}}_{ij}, \mathbf{u}_i, \mathbf{u}_j)}{\sigma_0} = \left[1 - \frac{\chi}{2}\left(\frac{(\hat{\mathbf{r}}_{ij}\cdot\mathbf{u}_i + \hat{\mathbf{r}}_{ij}\cdot\mathbf{u}_j)^2}{1 + \chi(\mathbf{u}_i\cdot\mathbf{u}_j)} + \frac{(\hat{\mathbf{r}}_{ij}\cdot\mathbf{u}_i - \hat{\mathbf{r}}_{ij}\cdot\mathbf{u}_j)^2}{1 - \chi(\mathbf{u}_i\cdot\mathbf{u}_j)}\right)\right]^{-1/2}, \quad (3)$$

$$\frac{\varepsilon(\hat{\mathbf{r}}_{ij}, \mathbf{u}_i, \mathbf{u}_j)}{\epsilon_0} = [\epsilon_1(\mathbf{u}_i, \mathbf{u}_j)]^{\nu} \times [\epsilon_2(\hat{\mathbf{r}}_{ij}, \mathbf{u}_i, \mathbf{u}_j)]^{\mu}, \quad (4)$$

where

$$\epsilon_1(\mathbf{u}_i, \mathbf{u}_j) = [1 - \chi^2(\mathbf{u}_i\cdot\mathbf{u}_j)^2]^{-1/2} \quad (5)$$

$$\epsilon_2(\hat{\mathbf{r}}_{ij}, \mathbf{u}_i, \mathbf{u}_j) = 1 - \frac{\chi'}{2}\left[\frac{(\hat{\mathbf{r}}_{ij}\cdot\mathbf{u}_i + \hat{\mathbf{r}}_{ij}\cdot\mathbf{u}_j)^2}{1 + \chi'(\mathbf{u}_i\cdot\mathbf{u}_j)} + \frac{(\hat{\mathbf{r}}_{ij}\cdot\mathbf{u}_i - \hat{\mathbf{r}}_{ij}\cdot\mathbf{u}_j)^2}{1 - \chi'(\mathbf{u}_i\cdot\mathbf{u}_j)}\right] \quad (6)$$

with $\chi = (\kappa^2 - 1)/(\kappa^2 + 1)$ and $\chi' = [(\kappa')^{1/\mu} - 1]/[(\kappa')^{1/\mu} + 1]$. As in the original paper of Gay and Berne,[38] we choose $\mu = 2$ and $\nu = 1$. Fixing these parameters leaves an interaction potential that depends on the additional two parameters, κ and κ'. κ is a measure of the length-to-breadth ratio of the particle. As a result, $\kappa > 1$ corresponds to prolate particles while $\kappa < 1$ corresponds to oblate particles. κ' plays an important role in the formation of ordered phases, as it determines the relative importance of side-by-side over end-to-end configurations. Consistent with this, Gibbs ensemble[39] and Gibbs-Duhem[40,41] Monte Carlo simulations for $\kappa = 3$ find that for high κ', the smectic B phase is the dominant ordered phase of the Gay-Berne fluid.[37] The nematic phase, in this case, is only stable at temperatures well above the liquid-vapor critical temperature, T_c, and for a narrow range of densities. By contrast, for low κ', the nematic phase is stable well below the liquid-vapor critical temperature and for a broader range of densities. In this case, the nematic phase can coexist with a vapor phase within the temperature range: $T_2 < T < T_1$, where T_1 is the temperature of the vapor-liquid-nematic triple point and T_2 is the temperature of the vapor-nematic-smectic B triple point. A suitable selection of κ' for the elongation considered in these simulations, $\kappa = 3$, thus enables coexistence of nematic and vapor phases. Unfortunately, results for other values of κ are not available in the literature.

We note that with our parametrization, the Gay-Berne molecules show planar anchoring in the vapor-nematic interface.[42] However, by using other set of Gay-Berne parameters, homeotropic anchoring can be promoted.[33,43,44] This has also been observed in lattice liquid crystal models.[45]

B. Simulation procedure to generate nematic drops

Our most realistic representation of a nematic drop without shape constraints consists of a large enough amount of nematic phase in equilibrium with its vapor. The Gay-Berne phase behavior provides natural ways to achieve this for $\kappa = 3$ and low κ'. We follow existent simulation work[37] and perform isothermal-isobaric Monte Carlo simulations ($NPT - \mathrm{MC}$) to generate a nematic phase right on the nematic-vapor coexistence curve. We could perform additional simulations of this type to map the phase boundaries for other values of κ. However, we have chosen an alternative, faster route based on the so called "zero-pressure" simulation.[46] The method consists in locating the system in a region of the phase diagram with $T_2 < T < T_1$ and with a density that is larger than the nematic-vapor coexistence density at the selected temperature. By performing $NPT - \mathrm{MC}$ computer simulations at $P = 0$, the system evolves towards decreasing its density, but in the process it encounters the nematic-vapor coexistence curve. If the simulations are short, we prevent the system from undergoing large fluctuations in volume, and the system is forced to remain right at the coexistence curve at the nematic density. We achieve this by selecting a maximum trial volume change, ΔV, that is small enough but adjusted to get a volume change acceptance ratio of about 30%. A snapshot of the system in this situation is shown in the top panel of Fig. 1 for $\kappa = 4$, $\kappa' = 0.5$, and $T = 1.00$. Hereafter we use reduced units, where T is in units of ϵ_0/k_B. By modifying the values of T and κ', we are able to find other situations

FIG. 1. Snapshots of the MC simulations for $\kappa = 4$, $\kappa' = 1$, and $T = 0.5$. The top panel corresponds to the $NPT -$ MC bulk simulations for $P = 0.0$. The bottom panel is obtained in the subsequent NVT simulations (see text). In this case a nematic drop forms in coexistence with its vapor.

of nematic-vapor equilibrium. We follow this approach for $\kappa = 4$ and $\kappa = 6$. For $\kappa = 3$, we use existent simulation results to find the values of T, for $\kappa' = 1$, where the nematic coexists with its vapor. We summarize all the parametric situations used in our studies in Table I, and emphasize we always use a fixed number of particles of $N = 4000$.

When the final configuration of these "zero pressure" simulations is reached, we significantly enlarge the simulation box and perform additional $NVT -$ MC simulations to allow the system to equilibrate with its vapor. This provides the desired nematic drop in coexistence with its vapor, as shown in the bottom panel of Fig. 1 and also in Figs. 2 and 3 for different values of κ, κ' and T. Very long runs are necessary to stabilize the drops; in all the three cases shown in Figs. 1–3, we needed more than 10^7 cycles, where each cycle consists of N attempted particle translations and rotations. We also note that since we use periodic boundary conditions, the volume of the simulation box must be large enough to prevent interactions between particles in the drop with their periodic images, but small enough to prevent a large number of molecules from escaping from the drop to the vapor phase. Nevertheless, the latter constraint is not dramatic due to the small density of the vapor phase compared to the density of the corresponding coexisting isotropic liquid or nematic phase; note that all considered temperatures are well below the vapor-isotropic critical point. In fact, for all the considered cases, less than 10% of the particles are in the vapor, with all drops having essentially the same number of particles.

TABLE I. Phase states considered in this work, and eccentricities corresponding to the drops generated under the indicated conditions.

κ	κ'	T	Phase	e
3	1.0	0.66	Isotropic	1.02(1)
3	1.0	0.59	Nematic	1.38(1)
3	1.0	0.55	Nematic	1.46(1)
4	1.0	0.70	Nematic	1.68(1)
4	1.0	0.60	Nematic	1.82(1)
4	1.0	0.50	Nematic	1.94(1)
4	0.5	1.40	Nematic	1.39(1)
4	0.5	1.30	Nematic	1.51(1)
4	0.5	1.20	Nematic	1.65(1)
4	0.5	1.10	Nematic	1.90(1)
4	0.5	1.00	Nematic	2.04(1)
6	0.5	1.60	Nematic	2.10(2)
6	0.5	1.50	Nematic	2.14(2)
6	0.5	1.40	Nematic	2.20(2)
6	0.5	1.30	Nematic	2.22(1)
6	0.5	1.20	Nematic	2.24(1)
6	0.5	1.10	Nematic	2.26(3)
6	0.5	1.00	Nematic	2.28(1)

We note that we choose low values of κ', as in this situation the nematic-vapor coexistence region is larger. It is then easier in this case to obtain nematic droplets coexisting with its vapor, which is what we are interested in studying from a simulation point of view.

C. Calculating drop shape and nematic order

To characterize the shape of the drops, we calculate the inertial tensor and diagonalize it to obtain its eigenvalues and

FIG. 2. Drop snapshot for $\kappa = 3$, $\kappa' = 1$, and $T = 0.55$.

FIG. 3. Drop snapshot for $\kappa = 6$, $\kappa' = 0.5$, and $T = 1.5$.

principal moments of inertia: I_1, I_2, and I_3, expressed in units of $m\sigma_0^2$, with m the mass of a molecule.

To compare the shapes of different drops, we calculate the eccentricity, e. Assuming an ellipsoidal shape:

$$e = \sqrt{\frac{I_1 + I_2}{I_3} - 1}, \tag{7}$$

where I_3 is the lowest principal moment of inertia of all three, as shown in the schematic of Fig. 4.

We quantify the global nematic ordering by first calculating the tensor order parameter:

$$Q = \left\langle \frac{1}{N} \sum_{i=1}^{N} \frac{3\mathbf{u}_i \otimes \mathbf{u}_i - I}{2} \right\rangle \tag{8}$$

and by then choosing the larger positive eigenvalue of the tensor order parameter, S, as the representative measure of the global nematic order. We note that, with this selection, the director of the phase would correspond to the associated eigenvector, **n**.

We also characterize the shape and nematic texture within the drop by calculating density and orientational profiles. We divide the drop along its major axis, which we label z, into circular rings of width Δz. Every slice is further divided into circular shells of average radius r and width Δr. By counting the number of particles within each shell, we obtain the density profile, $\rho(r, z)$:

$$\rho(r, z) \equiv \frac{1}{2\pi r} \left\langle \sum_{i=1}^{N} \delta(z_i - z)\delta(r_i - r) \right\rangle, \tag{9}$$

where (r_i, z_i) are, respectively, the instantaneous radial and axial coordinates of particle i. As usual, we present a reduced density profile in units of σ_0^{-3}, and all distances in units of σ_0. The orientational profile is obtained by calculating the orientational order profile $\rho_2(r, z)$, defined as the averaged second order Legendre polynomial:

$$\rho_2(r, z) \equiv \frac{1}{2\pi r \rho(r, z)} \left\langle \sum_{i=1}^{N} \left(\frac{3\cos^2\theta_i - 1}{2} \right) \delta(z_i - z)\delta(r_i - r) \right\rangle, \tag{10}$$

where θ_i is the angle between the major axis of molecule i and the nematic director, **n**.

III. RESULTS AND DISCUSSION

We find different values of the principal moments of inertia depending on the length-to-breadth ratio of the nematogens. For instance, for $\kappa = 3$ and $T = 0.55$, we find $I_1 = 108 \pm 1$, $I_2 = 111 \pm 1$, and $I_3 = 70 \pm 1$, while for $\kappa = 4$ and $T = 1.20$, we find $I_1 = 143 \pm 2$, $I_2 = 137 \pm 2$, and $I_3 = 75 \pm 2$. As a result, $I_1 \approx I_2 \neq I_3$, indicating the drops essentially have an axisymmetric shape. Furthermore, since I_3 is the smallest of the three principal moments of inertia, the drops are essentially prolate ellipsoids, consistent with the schematic of Fig. 4; this is true for all simulated nematic droplets. However, for a given κ' and T, the droplet eccentricity increases with κ, as shown in Table I. As a result, the drops become more elongated as the length-to-breadth ratio of the molecules increases.

We also find that **n** is parallel to the eigenvector associated to the smallest principal moment of inertia, **d**, which provides the direction of the major axis of the drop, as shown in Fig. 5. This indicates the nematic director lies along the major axis of the drops; this is true for all values of κ, κ', and

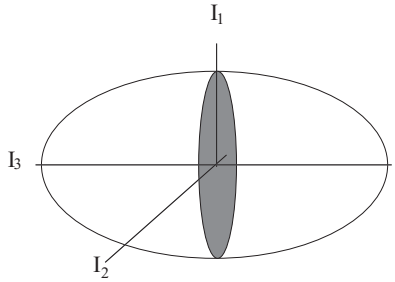

FIG. 4. Scheme of the nematic drop, where the association of the principal moments of inertia with the principal axes of the drop is highlighted.

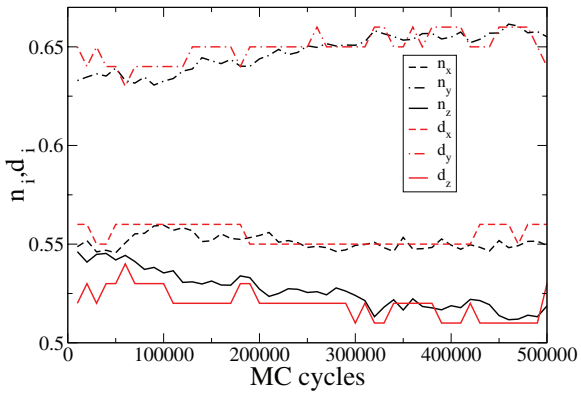

FIG. 5. Components of the nematic director and the eigenvector associated to the smallest eigenvalue of the inertial tensor for $\kappa = 4$ and $T^* = 1.00$.

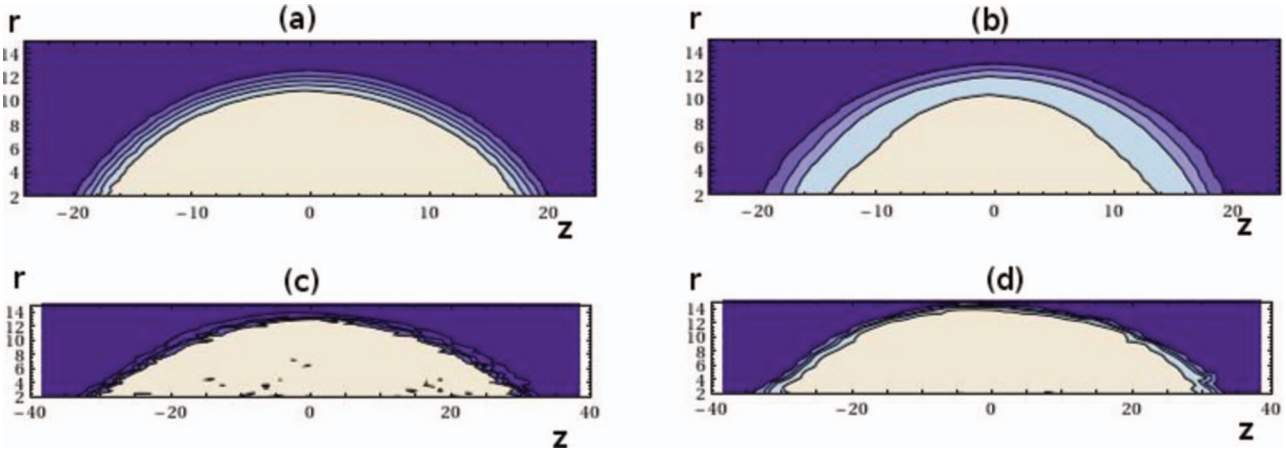

FIG. 6. Contour plots for the (a) and (c) density and (b) and (d) orientational order profiles for (a) and (b) $\kappa = 3$, $\kappa' = 1$, $T = 0.55$ and (c) and (d) $\kappa = 6$, $\kappa' = 0.5$, $T = 1.1$. The density contours correspond to reduced densities in units of σ_0^{-3} ranging from 0.25 to 0.05 in (a) and from 0.10 to 0.02 in (c). The orientational order contours correspond to values of ρ_2 from 0.7 to 0.1.

T in Table I. Furthermore, we find that this direction remains almost unchanged throughout the simulation after the initial equilibration period.

Let us consider in detail the case $\kappa = 3$, $\kappa' = 1$. For high temperatures, above the vapor-isotropic-nematic triple point, but below the vapor-isotropic critical point, drops are expected to be isotropic. Consistent with this, our simulations for $T = 0.66$ result in the formation of a drop with $e = 1.02$, as shown in Table I. In addition, the orientational order is negligible everywhere inside the drop. As a result, $K = 0$ and the shape is solely determined by surface tension. By contrast, for a temperature of $T = 0.55$, which is below the vapor-isotropic-nematic triple point, the resultant drop exhibits nematic ordering and an eccentricity of $e = 1.48$. Visual inspection of drop snapshots (see Fig. 2) shows that the molecules orient preferentially along the major axis of the drop and tangentially at the nematic-vapor interface. However, near the end of the drop along its major axis, the nematic order is lost to a large extent: this is an indication of the presence of the two boojums required for topological reasons, which as expected, maximize their separation by locating themselves along the major axis of the droplet. Thus, in this case, the drop is of bipolar character.

To characterize more quantitatively our results, we analyze the density and orientational order profiles. Figures 6(a) and 6(b) show the contour plots for ρ and ρ_2, respectively. On the one hand, the density profile confirms that the drop shape is nearly elliptical, with ρ approaching its value in the vapor phase in a narrow region close to the drop boundary. On the other hand, the orientational profiles indicate that the orientational order is very different in the equatorial plane and near the poles of the drop. Figure 7 shows the projections of the density and orientational order profiles in the equatorial plane ($z = 0$) and near the poles ($z = \pm 18$). For $z = 0$, both ρ and ρ_2 take maximum and constant values of $\rho \sim 0.3$ and $\rho_2 \sim 0.8$ up to the nematic-vapor interface of the drop. At this point both ρ and ρ_2 simultaneously decay down to their bulk vapor values. However, near the edges of the drop, for $z = \pm 18$, near its major axis, $r = 2$, the orientational order shows a major reduction to values slightly below 0.2; this is consistent with the presence of the surface boojums of the drop.

As κ is increased, we observe that the shape of the drop changes to a spindle-like shape (see Figs. 1 and 3). This is indeed confirmed by the analysis of the density and orientational order parameter contour plots in Figs. 6(c) and 6(d) for $\kappa = 6$. In these cases, we find that the isodensity lines are much straighter near the drop edges compared to the $\kappa = 3$ case [see Figs. 6(c) and 6(d)]. In addition, there is a change in the nematic texture as the molecules close to the edges now are oriented preferentially along the main axis of the drop, which is characteristic for an almost homogeneous nematic texture. The differences between drops with different κ are easier to appreciate by plotting the density and the orientational order parameter profiles corresponding to the center ($z = 0$) and edges of the drop. As for the $\kappa = 3$ case shown previously, for $z = 0$, both ρ and ρ_2 take their maximum values, as expected. Near the edges, however, we observe that the orientational order progressively increases with κ; $\rho_2 \sim 0.2$ for $\kappa = 3$, as shown in Fig. 7, $\rho_2 \sim 0.3$–0.4 for $\kappa = 4$, as shown in Fig. 8, and $\rho_2 \sim 0.8$ for $\kappa = 6$, as shown in Fig. 9. This

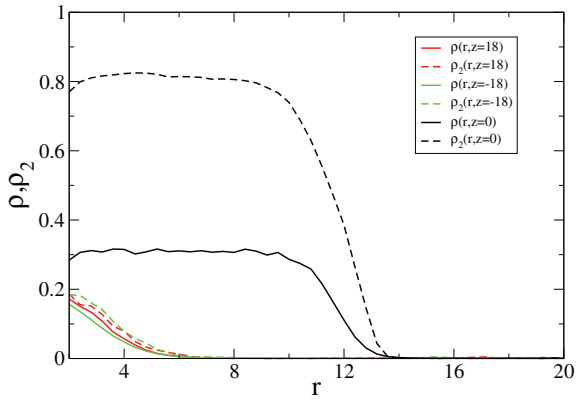

FIG. 7. Density and orientational order profiles at the center ($z = 0$) and near the edges of a drop for $\kappa = 3$, $\kappa' = 1$, and $T = 0.55$. All distances are in units of σ_0.

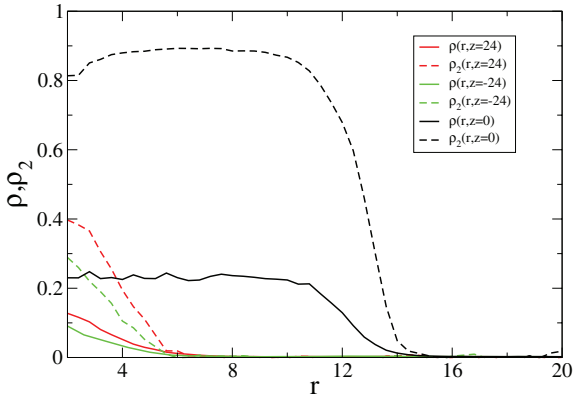

FIG. 8. The same as Fig. 7 for $\kappa = 4$, $\kappa' = 1$, and $T = 0.7$.

indicates that with increasing κ, there is a crossover from a bipolar texture to an almost homogeneous texture, driven by the increase of the drop eccentricity. The drop thus transitions from spheroidal to spindle-like for sufficiently large values of κ.

This trend is consistent with expectations from continuum theory, if the Frank elastic constants increase with increasing κ. In this case, Δ would decrease, provided the interfacial tension remains unaltered, resulting in more elongated droplets. However, the values of K for Gay-Berne simulations have only been calculated for $\kappa = 3$.[47,48] As a result, it is not known at this stage if K changes with κ and/or the form of this dependence. Furthermore, the values of K from these simulations correspond to bulk materials and it is not obvious whether these will change as the system size decreases. Similarly, for the interfacial tension, it is also not known whether it changes or not with κ; the only available values of γ are known for the single case of $\kappa = 3$.[49] In this case, however, there is evidence from Lennard-Jones simulations that γ depends on whether the interface is planar or spherical.[50] All these facts prevent a direct comparison between our simulation results and expectations based on continuum model approaches; this would require the calculation of the Frank elastic constants and interfacial tension as a function of κ, for systems of different size with boundaries of different curvature.

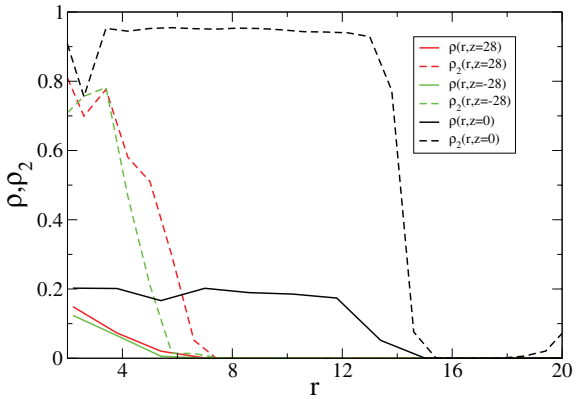

FIG. 9. The same as Fig. 7 for $\kappa = 6$, $\kappa' = 0.5$, and $T = 1.1$.

IV. CONCLUSIONS

We have performed computer simulations of nematic drops composed of interacting Gay-Berne rod-like molecules in coexistence with their vapor. We find that the drops are in general non-spherical, but elongated. For small length-to-breadth ratio of the molecules, κ, the drops are ellipsoidal-like and the nematic texture in the drop is bipolar. The topologically required boojums maximize their distance and arrange themselves on the surface of the drop along the major axis of the ellipsoid, with a director field that is on average parallel to this axis. We find that increasing κ results in more elongated drops, with a spindle-like shape characterized by the presence of cusps at both poles of the drop and a nematic texture reminiscent of an almost homogeneous state. The transition from the bipolar to the homogeneous configuration of the drop seems to be smooth, in agreement with theoretical predictions[15,16] and similar to that observed for mixtures of hard rods and spheres.[36] However, the absence of good estimates for surface tensions and elastic constants in the Gay-Berne model prevents a direct comparison of our simulation results with theoretical expectations. Nevertheless, our results can serve as the starting point for additional studies, for example, in the presence of external forces.

ACKNOWLEDGMENTS

L.F.R. wishes to thank Professor van der Schoot for helpful comments. L.F.R. and J.M.R.-E. acknowledge financial support from the Spanish MICINN through Grant No. FIS2009-09326, and Junta de Andalucía through Grant No. P09-FQM-4938, both co-funded by the EU FEDER. A.F-N. thanks NSF for CAREER Award DMR-0847304.

[1] P. S. Drzaic, *Liquid Crystal Dispersions* (World Scientific, Singapore, 1995).
[2] D. Rudhardt, A. Fernandez-Nieves, D. R. Link, and D. A. Weitz, Appl. Phys. Lett. **82**, 2610 (2003).
[3] A. Fernandez-Nieves, D. R. Link, and D. A. Weitz, Appl. Phys. Lett. **88**, 121911 (2006).
[4] R. L. Sutherland, V. P. Tondiglia, L. V. Natarajan, T. J. Bunning, and W. W. Adams, Appl. Phys. Lett. **64**, 1074 (1994); T. J. Bunning, L. V. Natarajan, V. P. Tondiglia, and R. L. Sutherland, Annu. Rev. Mater. Sci. **30**, 83 (2000).
[5] C. C. Bowley, P. A. Kossyrev, G. P. Crawford, and S. Faris, Appl. Phys. Lett. **79**, 9 (2001); M. Jazbinsek, I. Drevensek, M. Zgonik, A. K. Fontecchio, and G. P. Crawford, J. Appl. Phys. **90**, 3831 (2001).
[6] J. D. Bernal and I. Fankuchen, J. Gen. Physiol. **25**, 111 (1941).
[7] A. S. Sonin, Colloid J. USSR **60**, 129 (1998).
[8] B. I. Lev, V. G. Nazarenko, A. B. Nych, D. Schur, P. M. Tomchuk, J. Yamamoto, and H. Yokoyama, Phys. Rev. E **64**, 021706 (2001).
[9] C. Herring, Phys. Rev. **82**, 87 (1951).
[10] S. Chandrasekhar, Mol. Cryst. **2**, 71 (1966).
[11] R. D. Williams, Rutherford Appleton Laboratory Report No. RAL-85-028, 1985 (unpublished).
[12] E. G. Virga, *Variational Theories for Liquid Crystals* (Chapman and Hall, London, 1994).
[13] A. V. Kaznacheev, M. M. Bogdanov, and S. A. Taraskin, J. Exp. Theor. Phys. **95**, 57 (2002).
[14] A. V. Kaznacheev, M. M. Bogdanov, and A. S. Sonin, J. Exp. Theor. Phys. **97**, 1159 (2003).
[15] P. Prinsen and P. van der Schoot, Phys. Rev. E **68**, 021701 (2003).
[16] P. Prinsen and P. van der Schoot, Eur. Phys. J. E **13**, 35 (2004).
[17] J. S. Rowlinson and B. Widom, *Molecular Theory of Capillary* (Oxford University Press, Oxford, 1982).
[18] J. S. Rowlinson, J. Phys.: Condens. Matter **6**, A1–A8 (1994).

[19]S. M. Thompson, K. E. Gubbins, J. P. R. B. Walton, R. A. R. Chantry, and J. S. Rowlinson, J. Chem. Phys. **81**, 530 (1984).
[20]A. G. Meyra, G. J. Zarragaicoechea, and V. Kuz, Fluid Phase Equilib. **235**, 191 (2005).
[21]K. Laasonen, S. Wonczak, R. Strey, and A. Laaksonen, J. Chem. Phys. **113**, 9741 (2000).
[22]K. Yasuoka and M. Matsumoto, J. Chem. Phys. **109**, 8451 (1998).
[23]S. Toxvaerd, J. Chem. Phys. **115**, 8913 (2001).
[24]A. P. Shreve, J. P. R. B. Walton, and K. E. Gubbins, J. Chem. Phys. **85**, 2178 (1986).
[25]V. V. Zakharov, E. N. Brodskaya, and A. Laaksonen, J. Chem. Phys. **107**, 10675 (1997).
[26]L. G. Macdowell, V. K. Shen, and J. R. Errignton, J. Chem. Phys. **125**, 034705 (2006).
[27]M. Salonen, I. Napari, and H. Vehkamaki, Mol. Simul. **33**, 15 (2007).
[28]Y. Trukhina and T. Schilling, Phys. Rev. E **77**, 011701 (2008).
[29]W. Huang and G. F. Tuthill, Phys. Rev. E **49**, 570 (1994).
[30]J. Dzubiella, M. Schmidt, and H. Lowen, Phys. Rev. E **62**, 5081 (2000).
[31]A. P. J. Emerson and C. Zannoni, J. Chem. Soc., Faraday Trans. **91**, 3441 (1995).
[32]M. Tsige, M. P. Mahajan, C. Rosenblatt, and P. L. Taylor, Phys. Rev. E **60**, 638 (1999).
[33]M. A. Bates and G. R. Luckhurst, Struct. Bonding (Berlin) **94**, 65 (1999).
[34]M. A. Bates, Chem. Phys. Lett. **368**, 87 (2003).
[35]R Berardi, A. Conatantini, L. Mucioli, S. Orlandi, and C. Zannoni, J. Chem. Phys. **126**, 044905 (2007).
[36]Y. Trukhina, S. Jungblut, P. van der Schoot, and T. Schilling, J. Chem. Phys. **130**, 164513 (2009).
[37]E. de Miguel, E. Martin del Rio, J. T. Brown, and M. P. Allen, J. Chem. Phys. **105**, 4234 (1996).
[38]J. G. Gay and B. J. Berne, J. Chem. Phys. **74**, 3316 (1981).
[39]A. Z. Panagiotopoulos, Mol. Phys. **61**, 813 (1987).
[40]D. A. Kofke, Mol. Phys. **78**, 1331 (1993).
[41]M. Dijkstra and D. Frenkel, Phys. Rev. E **51**, 5891 (1995).
[42]E. Martin del Rio and E. de Miguel, Phys. Rev. E **55**, 2916 (1997).
[43]E. Martin del Rio, E. de Miguel, and L. F. Rull, Physica A **213**, 138 (1995).
[44]E. de Miguel and E. Martin del Rio, Int. J. Mod. Phys. C **10**, 431 (1999).
[45]M. A. Bates, Phys. Rev. E **65**, 041706 (2002).
[46]D. Frenkel and B. Smit, *Understanding Molecular Simulation, from Algorithms to Applications* (Academic, 2002).
[47]M. P. Allen, M. A. Warren, M. R. Wilson, A. Sauron, and W. Smith, J. Chem. Phys. **105**, 2850 (1996).
[48]N. H. Phuong, G. Germano, and F. Schmid, J. Chem. Phys. **115**, 7227 (2001).
[49]E. de Miguel, J. Phys. Chem. B **112**, 4674 (2008).
[50]J. G. Sampayo, A. Malijevsky, E. A. Müller, E. de Miguel, and G. Jackson, J. Chem. Phys. **132**, 141101 (2010).